Medicinal Chemistry Research (2023) 32:682–693
https://doi.org/10.1007/s00044-023-03028-8

MEDICINAL CHEMISTRY RESEARCH

ORIGINAL RESEARCH

Screening a small hydrazide-hydrazone combinatorial library for targeting the STAT3 in monocyte-macrophages with insulated reporter transposons

Valeri V. Mossine[1,2] · Steven P. Kelley[3] · James K. Waters[2] · Thomas P. Mawhinney[1,2,4]

Received: 30 December 2022 / Accepted: 1 February 2023 / Published online: 13 February 2023

Abstract

The Signal Transducer and Activator of Transcription 3 (STAT3) pharmacological targeting is regarded as a prospective approach to treat cancer, autoimmune disorders, or inflammatory diseases. We have developed a series of reporters of the STAT3, NF-κB, Nrf2, metal-responsive transcription factor-1 (MTF-1), and hypoxia-inducible factor 1α (HIF-1α) transcriptional activation in human monocyte-macrophage line THP-1. The reporter lines were employed to test a set of hydrazide-hydrazones as potential STAT3 inhibitors. A hydrazide-hydrazone library composed of 70 binary combinations of 7 carbonyl and 10 hydrazide components, including a STAT3 inhibitor clinical drug nifuroxazide, has been assembled and screened by the reporters. For the library as a whole, significant correlations between responses of the STAT3 and NF-κB or the STAT3 and HIF-1α reporters in THP-1 monocytes were found. For selected inhibitory combinations, respective hydrazide-hydrazones have been prepared and tested individually. The most potent 2-acetylpyridine 4-chlorobenzoylhydrazone exhibited the STAT3 inhibitory potential significantly exceeding that of nifuroxazide (ED_{50} 2 vs 50 μM respectively) in THP-1 cells. We conclude that insulated reporter transposons could be a useful tool for drug discovery applications.

Graphical Abstract

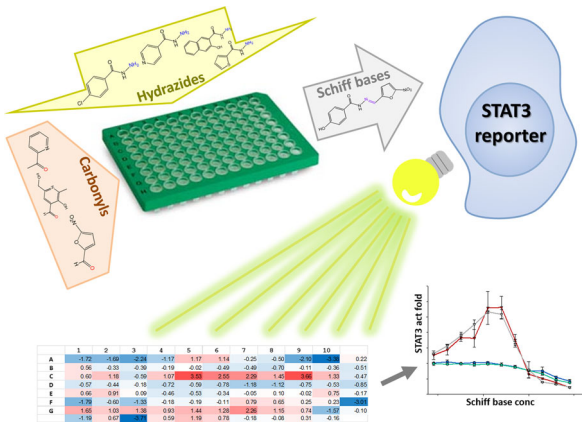

Supplementary information The online version contains supplementary material available at https://doi.org/10.1007/s00044-023-03028-8.

✉ Valeri V. Mossine
mossinev@missouri.edu

[1] Department of Biochemistry, University of Missouri, Columbia, MO 65211, USA

[2] Agriculture Experiment Station Chemical Laboratories, University of Missouri, Columbia, MO 65211, USA

[3] Department of Chemistry, University of Missouri, Columbia, MO 65211, USA

[4] Department of Child Health, University of Missouri, Columbia, MO 65211, USA

Keywords Schiff base · Cytotoxicity · Transcriptional factors · Crystal structure · Green fluorescent protein · Isoniazid

Introduction

Remarkable achievements of modern medicine have become possible, to some extent, due to advances in molecular biology and high-throughput screening techniques, which enabled target-specific drug discovery and development [1]. Nevertheless, persistent vulnerability of humankind to infections, cardiovascular diseases, cancer, or neurological disorders implies that there remains a great need in safer, more effective, and more affordable drugs [2]. To meet such a need, more efficient and less costly screening and evaluation approaches at early stages of drug discovery, such as multi-target profiling or drug repurposing [3, 4], could help.

Signal Transducer and Activator of Transcription 3 (STAT3) is a cytoplasmic inducible transcription factor which relays extracellular signals, typically provided by cytokines or growth factors, such as interleukin-6 (IL-6) or epidermal growth factor (EGF) [5]. The principal signaling pathway leading to activation of STAT3 involves recognition of IL-6 by a cytokine receptor, a subsequent activation of associated Janus tyrosine kinases (JAKs), phosphorylation of cytoplasmic STAT3 by JAK, and translocation of phosphorylated STAT3 to the nucleus, where it regulates gene expression. In turn, STAT3 induces the expression of a number of cytokines, chemokines and other factors which are known to support chronic inflammation, a major risk factor in oncogenesis [6]. Moreover, STAT3 upregulates a number of genes that are involved in cancer proliferation, invasion, and metastasis [5]. The involvement of this transcription factor in cancer cell immune evasion has been recognized, as well [7]. Thus, targeting the JAK/STAT3 pathway has been identified as a potentially important approach in cancer immunotherapies, and a significant effort was devoted to development of agents inhibiting the pathway. For example, direct-acting inhibitors of JAK2 ruxolitinib and fedratinib have been FDA approved for treatment of some leukemias, whereas a couple dozen more JAK and STAT3 inhibitors undergo clinical trials against various cancers [8]. In addition, a number of drugs, currently in clinical use, have been indicated for repositioning as inhibitors of the JAK/STAT3 pathway in cancer [9]. For instance, nifuroxazide, a synthetic antibacterial used in treatment of infectious diarrheas, has been identified 15 years ago as a potent inhibitor of STAT3 [10], with efficacy against experimental melanoma [11], pulmonary fibrosis [12], hepatocellular carcinoma [13], or inflammatory conditions in diabetic kidney [14].

Nifuroxazide structure is 5-nitro-2-furaldehyde 4-hydroxybenzhydrazone, a representative of a vast class of aromatic hydrazide-hydrazones, a subclass of Schiff bases, which are widely used in medicinal chemistry [15]. In addition to nifuroxazide, many hydrazide-hydrazones were proposed as potential anti-inflammatory or anti-cancer agents [16, 17]. Because of well-known lability of the azomethine bond in hydrazide-hydrazones, their therapeutic effects may not necessarily be attributed to the Schiff base structures, due to hydrolysis or cross-reaction with endogenous carbonyls in the cellular milieu. For drug discovery, however, the "bioactivity first, mechanism later" approach may be preferred in high-throughput screening of large libraries or screening biological extracts, whereby defined structure-driven search would be suboptimal. Nifuroxazide and a number of other therapeutic drugs that contain azomethine bond [15], may be prepared readily in biocompatible solvents in high yield via condensation reaction between acyl hydrazide and carbonyl components, thus skipping individual isolation of the drug candidates in such "combinatorial library" before testing in biological models.

Recently, we have developed a series of insulated reporter transposons for evaluation of the inflammation- and cellular stress-relevant signaling pathways [18]. Introduction of these reporters into genomes of immortalized cell lines allowed for generation of stable reporter cell lines suitable for functional characterization of bioactive molecules, such as flavonoids, in a middle- to high-throughput fashion [19]. Here, we communicate results of testing a stable THP-1 monocyte-macrophage based reporters of the JAK/STAT3 pathway and four other cell signaling pathways for screening a small combinatorial library of hydrazide-hydrazones structurally related to nifuroxazide.

Results and discussion

Validation of reporters

To generate new reporter cell lines, we employed previously assembled reporter plasmids which carry binding sites for the transcription factors STAT3 [19] and MTF-1 [20] that are flanked by the cHS4 insulators and inverted terminal repeats for recognition by the *piggyBac* transposase, as shown in Fig. 1A. The THP-1 monocytes, the HepG2 hepatocytes, and the NIH 3T3 murine embryonic fibroblasts were stably transfected with these plasmids, whereas the THP-1 based reporters for the transcriptional activity of NF-κB, Nrf2, and HIF-1α have been established

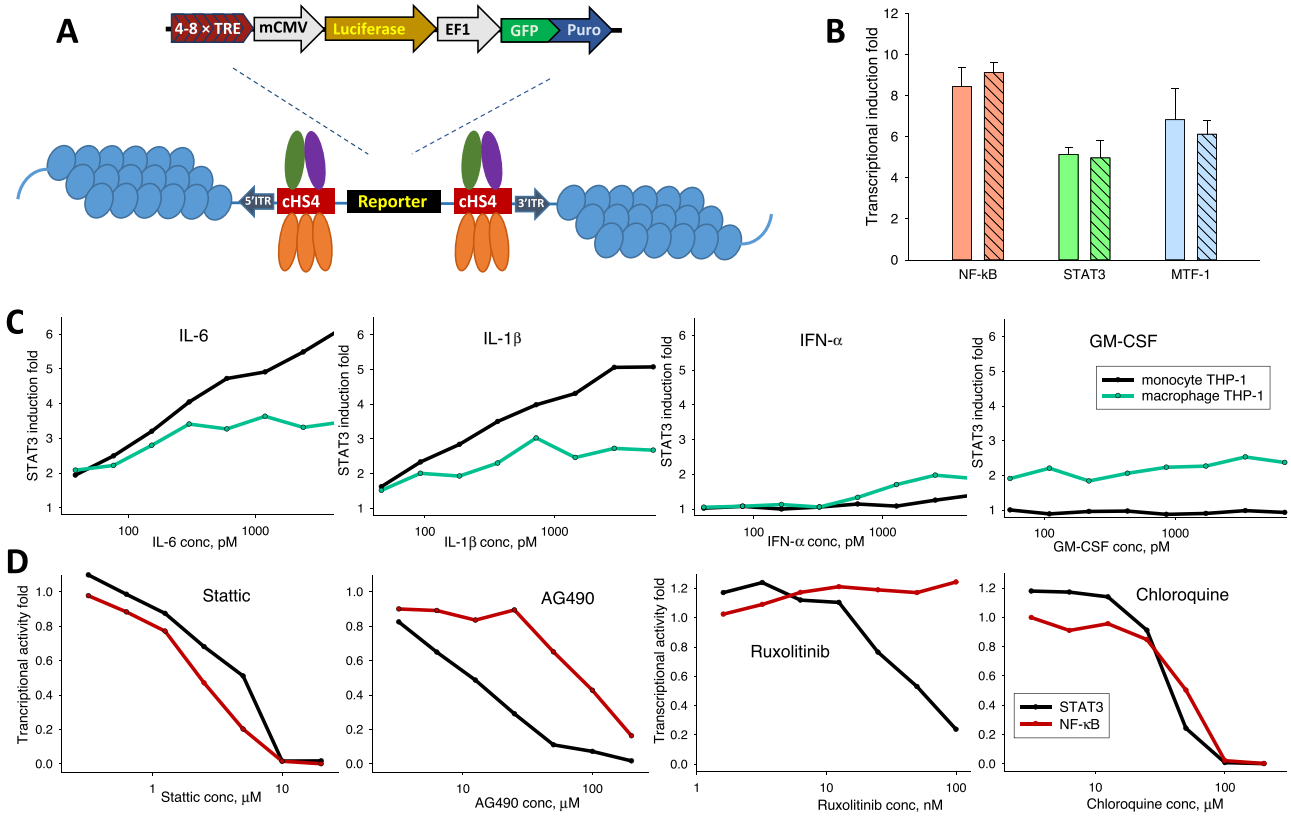

Fig. 1 Transcriptional activation assay in human monocyte-macrophage THP-1. **A** A general scheme of the reporter construct. Four to eight specific transcription factor binding sequences (transcription factor response elements, TREs) and the mCMV promoter regulate reporter firefly luciferase, while the EF1 promoter provides constant production of destabilized copepod GFP and puromycin resistance selector. The flanking insulators (core hypersensitive site 4, cHS4) protect from epigenetic silencing of the reporter, while the *piggyBac* transposon ITRs secure accurate and efficient insertion of the reporter into the genomic DNA. **B** Stability of the reporters in time. Comparative luciferase activity in reporter cells tested after 1 week (plainly colored bars) and 3 months (slanted fill pattern) that followed thawing of the cells. Reporters of the NF-κB, STAT3, and MTF-1 were treated for 16 h with 100 ng/mL LPS, 480 pM IL-6, and 100 μM $ZnSO_4$, respectively. The error bars are SDs, $n = 3$. **C** Comparison of responses to activators of the STAT3 in the non-differentiated monocytic and differentiated macrophage phenotypes of THP-1. **D** Comparison of responses to anti-inflammatory agents in THP-1 monocytes reporting the STAT3 or NF-κB activities. The data points in C and D are single measurements

earlier [18]. Keeping in mind that our goal in this study was to screen hydrazide-hydrazones for the STAT3 modulation and that hydrazide-hydrazones are established metal chelators [21], our choice of the TF reporter set was driven by implications of these TFs in oncogenic inflammatory processes and cellular responses to transition metals [22–25]. The new reporter cell lines were tested for stability and responsiveness to established inducers and inhibitors (Fig. 1). The functional activity of the STAT3 reporter did not change significantly within several weeks of culturing, it was not lost during differentiation of THP-1 monocytes into the macrophage phenotype, as well. However, there was a notable difference in responses to cytokines between the two phenotypes: while THP-1 monocytes were more sensitive to interleukins IL-6 and IL-1β, the STAT3 activation in response to interferon-α (IFNα) and granulocyte-macrophage colony-stimulating factor (GM-CSF) was more prominent in THP-1 macrophages (Fig. 1C). The basal activity of STAT3 in THP-1 monocytes decreased, dose-dependently, in presence of both inhibitors of JAK2 (AG490, ruxolitinib) and a direct STAT3 activation inhibitor (stattic), but also an autophagy inhibitor chloroquine (Fig. 1D).

Preparation and screening of the combinatorial library with the reporters of STAT3, NF-κB, Nrf2, HIF-1α, and MTF-1

The idea of hydrazide-hydrazone combinatorial library is based on the readiness of Schiff base formation between acyl hydrazides and sterically unhindered carbonyl groups in polar solvents, including water. We employed a DMSO/propylene glycol mixture as a solvent of choice, for reasons of low cytotoxicity, low volatility and good solubilizing capacity in respect to both reagents and products of the condensation reactions. In our hands, the Schiff base

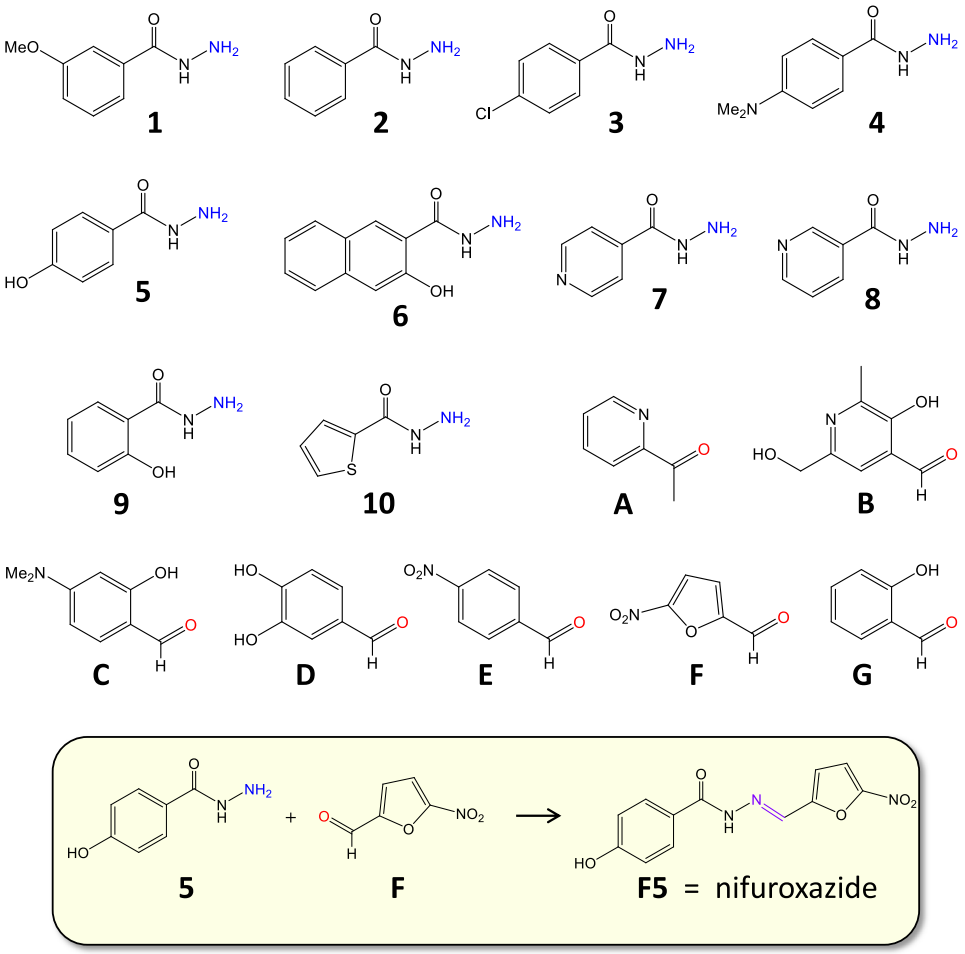

Fig. 2 Components of the combinatorial library and their codes. An example reaction of the Schiff base formation in the library is shown

formation between acyl hydrazides and aromatic aldehydes or 2-acetylpyridine was complete, as evidenced by TLC checkup, within 1–5 h at 55 °C. The library was assembled in a 96-well plate format, with 10 hydrazides and 7 carbonyl components coded, respectively, with the plate column numbers, **1** through **10**, and the row letters, **A** through **G**, as shown in Fig. 2. The unreacted hydrazides were located in the row H, the unreacted carbonyls were located in the column 11. The column 12 was reserved for untreated controls and blanks. Combinations producing particular Schiff bases were subsequently coded by the well addresses, such as **A2**, **C10**, **G5** etc.

In our reporter constructs, continuous expression of destabilized copepod GFP is driven by the EF1 promoter (Fig. 1A); the expressed cGFP is continuously degraded and, unlike EGFP, does not over-accumulate intracellularly and does not affect important signaling pathways such as NF-κB [26]. As a consequence, GFP fluorescence reads are proportional to current total transcriptional/ translational activity in cells and, as we have shown previously [19], well correlated with the cellular viability determined by the resazurin (alamarBlue) reduction assay. Hence, relative viability of cells in our assay could be assessed by simply GFP fluorescence measurements, immediately before addition of the luciferase substrate for further determination of the specific transcriptional factor activation in the cell lysates.

As shown in Fig. 3 and Supplementary Figs. S1–S8, viabilities of THP-1 reporter cells, treated with any of the hydrazide or carbonyl reagents or most of the combinations at 25 µM, were not different from the carrier-only (0.5% v/v) treated controls. Notable exceptions are several combinations of 2-acetylpyridine, 4-(dimethylamino)-2-hydroxybenzaldehyde, and 5-nitro-2-furaldehyde, which could decrease the cellular viability by more than 30%. In two instances, the combinations **C6** and **G6** produced relative GFP fluorescence reads well above unit (Figs. S3, S4, S5, and S7), a likely artefact of an intracellular agent accumulation.

Screening the library with reporters of the STAT3, NF-κB, Nrf2, HIF-1α, and MTF-1 transcriptional activities produced a series of patterns (Fig. 4, Supplementary Figs. S1–S10) with distinct features that are discussed below.

Treatment of THP-1 monocytes bearing the STAT3 reporter with 25 or 12.5 µM combinatorial library (Fig. 4

	1	2	3	4	5	6	7	8	9	10	
A	0.74	0.75	0.50	0.76	0.96	0.86	0.93	0.93	0.83	0.79	0.98
B	0.98	1.01	1.02	0.98	0.98	1.03	1.03	1.00	1.01	1.01	0.99
C	0.79	0.78	0.88	0.96	0.83	0.91	0.90	0.84	0.77	0.77	1.02
D	1.01	0.99	0.94	0.97	0.99	0.96	1.00	0.95	0.94	0.95	1.01
E	0.95	1.03	0.98	0.93	0.96	0.98	1.00	1.02	0.98	0.96	1.00
F	0.88	0.90	0.85	0.98	0.88	0.85	0.92	0.93	0.91	0.89	0.93
G	0.95	0.96	0.98	0.95	1.01	0.81	0.97	0.99	0.97	0.92	1.07
	1.00	1.00	1.02	1.01	1.02	0.99	1.00	1.00	0.98	0.97	

Fig. 3 Viabilities of the STAT3 reporter THP-1 monocytes treated with the combinatorial library at 25 µM for 16 h. The data points are single measurements

	1	2	3	4	5	6	7	8	9	10	
A	-2.65	-2.12	-3.52	-1.81	1.10	-0.67	0.04	-0.09	0.34	-1.57	0.06
B	-0.50	-0.48	-1.13	-0.09	-1.16	-0.25	-0.33	-0.41	-0.37	-0.49	-0.07
C	0.19	0.68	-1.54	-1.60	-0.95	-0.91	-0.54	0.24	-0.58	0.59	0.16
D	0.25	0.02	-0.33	0.42	-0.11	-0.28	-0.62	-0.46	0.11	0.56	-0.57
E	0.54	1.07	-0.08	0.05	0.10	-0.01	0.00	0.34	0.57	1.24	-0.08
F	-1.14	-0.57	-1.57	-0.02	-1.07	-0.30	-0.74	-0.61	-0.21	-0.70	-0.37
G	-0.43	-0.19	-0.38	0.08	0.37	-0.75	-0.95	-0.79	-0.30	-0.17	-0.11
	0.39	0.06	0.04	0.12	0.08	0.04	0.03	-0.08	0.03	0.13	

Fig. 4 Transcriptional activity of STAT3 in THP-1 monocytes treated with the combinatorial library at 25 µM for 16 h. The STAT3 activation is expressed as $\log_2$(r. a. f.), where r. a. f. = relative activation fold = luminescence in treated wells divided by luminescence in untreated controls. The data points are single measurements

and S1) revealed **A3** as clearly the most potent inhibitor of the basal STAT3 activity. Compared to nifuroxazide (**F5**), the inhibitory activity of **A3** was about 5 times stronger, in terms of the relative activation folds at these concentrations. In general, the majority of hydrazide-hydrazones were weak inhibitors of the basal STAT3 activity, and some, such as **A5** and **E10**, promoted weak activation of the STAT3. When the STAT3 pathway in THP-1 monocytes was activated with 240 pM interleukin-6, the luciferase activity increased about 5-fold (Fig. 1C), but the combinatorial library, at 25 µM, could counteract this increase to an extent that produced a pattern (Fig. S6) similar to that shown in Fig. 4. In fact, there was a good correlation between these two sets of responses, as shown in Fig. 5A. An equally good correlation was obtained when interleukin-1β was chosen as a STAT3 activator (Figs. S7, 5B), as well.

Next, we compared the STAT3 transcriptional responses to the library between THP-monocytes and THP-1 macrophages. In THP-1 macrophages, the cytotoxic and the STAT3 inhibitory effects of the library were less pronounced, as compared to the monocytes (Fig. S8), and the correlation between these two datasets (Fig. 5C) was not strong ($R^2 = 0.342$). Moreover, nifuroxazide and the rest of combinations containing 5-nitro-2-furaldehyde, and even this reagent alone, produced a pro-inflammatory effect of the STAT3 activation in the macrophages. All of the acylhydrazide reagents induced the STAT3 activation when presented to the macrophages, as well. Nevertheless, the combination **A3** retained the highest inhibitory potential against STAT3 within the library, with all but one combinations of 2-acetypyridine attenuating the basal STAT3 activity in the macrophages to some extent. In contrast, 25 µM **A3** was inducer of the STAT3 in human hepatocytes HepG2, with the **F9** taking the helm of the best STAT3 inhibitor (Fig. S9, Fig. 5D) in these cells, while in murine embryonal fibroblasts NIH 3T3, the **A3** retained its inhibitory activity against STAT3 activation, with p-chlorobenzoyl hydrazide (**3**) taking the lead as the strongest STAT3 pathway inhibitor (Fig. S10, Fig. 5E). There was no significant correlations between responses of the STAT3 reporters to the combinatorial library in THP-1 monocytes and HepG2 or NIH 3T3 cells ($R^2 = 0.069$ and 0.054, respectively). The nifuroxazide combination **F5** was inhibitory against the STAT3 in HepG2, but inactive against this transcription factor in NIH 3T3. On the final note, NIH 3T3 line was generally more sensitive to the combinatorial library than THP-1 cells, especially to the 2-acetylpyridine combinations (but not to 2-acetylpyridine alone), while the HepG2 cellular viabilities were generally unaffected in presence of the combinatorial library (Figs. S9 and S10).

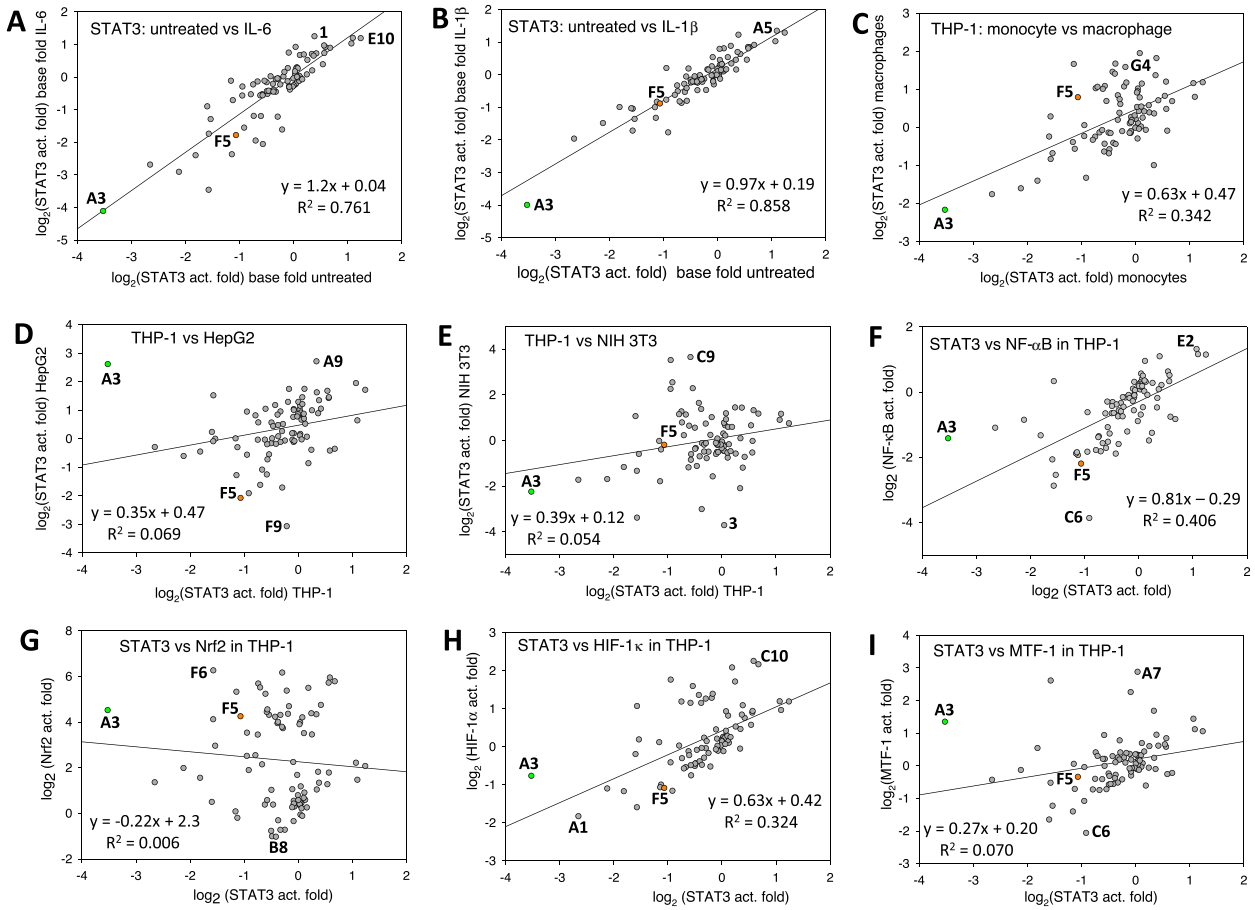

Fig. 5 Correlations between the transcriptional activities in THP-1 monocytes or macrophages, HepG2 hepatocytes, or NIH 3T3 murine embryonic fibroblasts, in response to the 25 μM combinatorial library for 16 h. In all graphs, datasets for abscissa are the same and expressed as $\log_2$(STAT3 activation fold), normalized for the basal STAT3 activity in untreated THP-1 monocytes. The STAT3 activation folds in datasets used for ordinates in the plots (**A**) and (**B**) were normalized for the STAT3 activity in THP-1 monocytes treated with IL-6 or IL-1β only. The transcriptional activation folds in datasets used for ordinates in the plots (**C**) through (**I**) were normalized for the basal transcriptional activities in untreated cells. Labeled are combinations **A3** (min abscissa value, green dot), **F5** (nifuroxazide, orange dot), **E10** (max abscissa value) and combinations with minimal and maximal values on the ordinate scale

We also compared transcriptional responses to the combinatorial library from the THP-1 reporters of five signaling pathways. The majority of the combinations, including **A3** and **F5**, inhibited the NF-κB pathway (Fig. S2), with the **C6** combination standing out as the best inhibitor. Responses from the NF-κB reporter correlated well with those recorded in the STAT3 reporter, as shown in Fig. 5F. In contrast, nearly all of the hydrazide and carbonyl reagents and their combinations induced the master regulator of the cellular stress and sensor of electrophilic species, transcription factor Nrf2 (Fig. S4). An exception to this trend were combinations of pyridoxal, but not pyridoxal alone. We found no correlation between responses to the library from the THP-1 reporters of STAT3 and Nrf2, as evidenced in Fig. 5G. The metal-sensitive transcription factors, HIF-1α and MTF-1, responded to the combinatorial library differentially. The activity hypoxia-inducible factor 1α was specifically enhanced by the majority of combinations of salicyladehyde and pyridoxal (Fig. S3). Notably, salicylaldehyde- and pyridoxal-derived hydrazide-hydrazones are well known biologically active chelators of iron(III) [27, 28], and activation of the HIF-1α is generally promoted by specific Fe(III) chelators, as well [29]. We also found a correlation between responses of the STAT3 and HIF-1α to the library, with $R^2 = 0.324$ (Fig. 5H). The zinc-sensitive transcription factor MTF-1, on the other hand, responded well to the combinations of 2-acetylpyridine (Figure S5), while the combinations of pyridoxal and 4-(dimethylamino)salicylaldehyde generally inhibited this transcription factor in THP-1 monocytes. There was no significant correlation between the STAT3 and MTF-1 responses to the library ($R^2 = 0.324$), as could be seen in Fig. 5I.

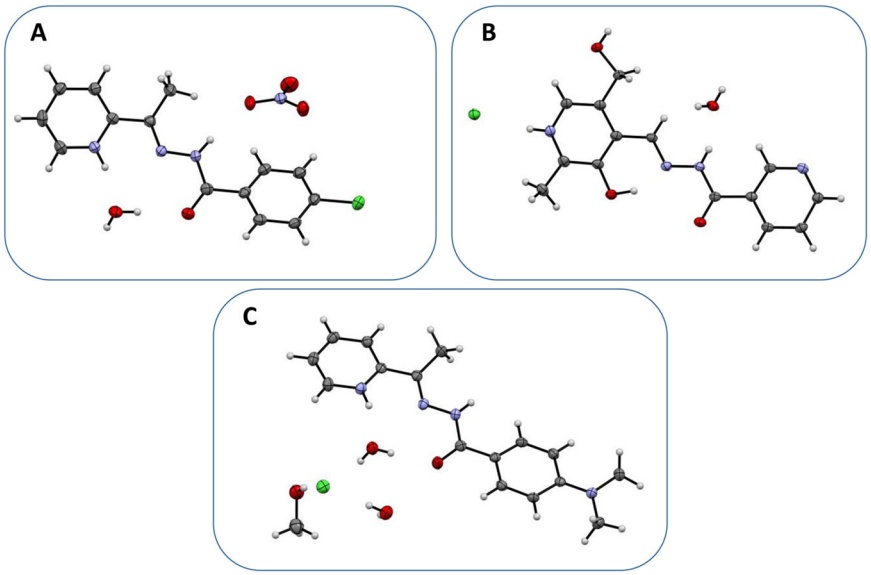

Fig. 6 Thermal ellipsoids at 50% probability for: **A** molecular structure of 2-acetylpyridine 4-chlorobenzoylhydrazone hydronitrate monohydrate (matches combination **A3**); (**B**) molecular structure of pyridoxal nicotinoylhydrazone hydrochloride monohydrate (matches combination **B8**); C. molecular structure of 2-acetylpyridine 4-dimethylaminobenzoylhydrazone hydrochloride dihydrate methanolic solvate (matches combination **A4**)

Comparison of the dose-dependent STAT3 inhibitory activity displayed by combinations and isolated hydrazide-hydrazones

In order to contest the functional identity of our combinatorial library with individually isolated hydrazide-hydrazones, we selected four combinations, **A3**, **A4**, **B8**, and **F5**. Thus, the **F5** combination was matched by a commercial sample of nifuroxazide, while for the rest of selected combinations, we prepared and structurally characterized respective synthetic hydrazide-hydrazones, namely 2-acetylpyridine 4-chlorobenzoylhydrazone (APypCBH), 2-acetylpyridine 4-dimethylaminobenzoylhydrazone (APyDMABH), and pyridoxal nicotinoylhydrazone (PNH) in form of their salts (Fig. 6, Fig. S11–S13). Crystallographic and structure parameters of these molecules are given in Table 1 and Tables S1–S9. In all three synthetic structures, the most basic nitrogen atoms resided on the carbonyl pyridine rings, while the hydrazide-hydrazone chain adopted the *trans* (*E*) configuration, similarly to reported conformations found in nifuroxazide solvates [30, 31].

We then measured the STAT3 activation folds in THP-1 monocytes treated with different concentrations of synthetic hydrazide-hydrazones and matching concentrations of the hydrazide/carbonyl combinations. The resulting dose-response curves are shown in Fig. 7. Clearly, the synthetic compounds and the matching combinations produced identical curves, signifying chemical identity of the combinations and the matching Schiff bases. One striking difference between nifuroxazide and the rest of tested hydrazide-hydrazones was the shape of dose-response curves. While nifuroxazide produced a typical sigmoid curve, the response curves from THP-1 monocytes to APypCBH, APyDMABH, and PNH were biphasic, with a maximum of the STAT3 activation reaching as high as threefold over the basal level. Thus, even though **A3**, **A4** and the matching hydrazide-hydrazones were better inhibitors of the STAT3 pathway than nifuroxazide at 25 μM concentration, at lower doses these combinations were rather pro-inflammatory, while their inhibitory activity at higher concentrations could be associated with their cytotoxic effects. In presence of IL-6, treatment with APypCBH produced a dose-response curve similar in shape to the curve obtained in the absence of this cytokine, thus suggesting a lack of significant synergistic or antagonistic interactions between IL-6 and APypCBH in the STAT3 reporter cells. Hence, in our hands, the dose profiling experiment singled out nifuroxazide as a pharmacological choice for further evaluation of its potential as a STAT3 inhibitor in immune cells, in accord with earlier findings by other research groups [10, 32].

Conclusions

This study demonstrated the utility of the insulated transcriptional activity reporter transposon for simultaneous monitoring of cytotoxic and anti-inflammatory effects of agents of interest in immune cells. Screening of 70 aromatic acylhydrazide/carbonyl combinations in five monocyte-macrophage based reporters of the inflammation-related signaling pathways allowed mapping potentially pro- and anti-inflammatory effects of these agents and exposed patterns of responses that were

Table 1 Crystallographic parameters of synthetic hydrazide-hydrazones

Molecule	1	2	3
CCDC code	2234388	2234387	2234389
Crystal data			
Chemical formula	$C_{14}H_{13}ClN_3O \times NO_3 \times H_2O$	$C_{16}H_{19}N_4O \times Cl \times 2(H_2O) \times CH_4O$	$C_{14}H_{15}N_4O_3 \times Cl \times H_2O$
M_r	354.75	386.87	195.19
Crystal system, space group	Orthorhombic, $P2_12_12_1$	Monoclinic, $P2_1/n$	Triclinic, $P\bar{1}$
Temperature (K)	150	150	100
a, b, c (Å)	7.0997 (7), 13.1368 (13), 16.4855 (16)	6.9109 (8), 15.3081 (16), 17.8913 (19)	5.9934 (5), 9.9511 (8), 13.4663 (10)
α, β, γ (°)	90, 90, 90	90, 92.463 (2), 90	91.208 (6), 93.702 (5), 104.811 (5)
V (Å^3)	1537.6 (3)	1891.0 (4)	774.25 (11)
Z	4	4	2
Radiation type	Mo $K\alpha$	Mo $K\alpha$	Cu $K\alpha$
μ (mm^{-1})	0.28	0.23	2.43
Crystal size (mm)	0.32 × 0.08 × 0.08	0.35 × 0.25 × 0.2	0.5 × 0.12 × 0.1
Data collection			
Diffractometer	Bruker *APEX* II area detector	Bruker *APEX* II area detector	Bruker X8 Prospector
Absorption correction	Multi-scan Bruker AXScale	Multi-scan Bruker AXScale	Multi-scan Bruker AXScale
T_{min}, T_{max}	0.692, 0.745	0.686, 0.746	0.600, 0.754
No. of measured, independent and observed [$I > 2\sigma(I)$] reflections	21573, 3173, 2626	27875, 4239, 3259	11958, 2982, 2743
R_{int}	0.055	0.044	0.046
θ_{max}, θ_{min} (°)	26.5, 2.0	27.3, 1.8	72.4, 3.3
Refinement			
$R[F^2 > 2\sigma(F^2)]$, $wR(F^2)$, S	0.034, 0.073, 1.02	0.022, 0.057, 1.08	0.044, 0.125, 1.06
No. of reflections	3173	4239	2982
No. of parameters	230	260	227
No. of restraints	2	0	0
H-atom treatment	H atoms treated by a mixture of independent and constrained refinement	H atoms treated by a mixture of independent and constrained refinement	H atoms treated by a mixture of independent and constrained refinement
$\Delta\rho_{max}$, $\Delta\rho_{min}$ (e Å^{-3})	0.21, −0.17	0.25, −0.28	0.51, −0.29
Absolute structure[37]	Flack x determined using 954 quotients [(I+)-(I-)]/[(I+)+(I-)]		
Absolute structure parameter	0.01 (3)		

consistent with nature of the carbonyl component in combinations. All selected hydrazide/carbonyl combinations and their matching hydrazide-hydrazone structures produced identical dose-response patterns in the STAT3 reporter cells. Thus, the carbonyl/amino combinatorial libraries deserve attention as an economical alternative to sets of synthetic Schiff bases. Results of this in vitro study may inform future laboratory and clinical studies aiming at nifuroxazide pharmacology, as well as the transcriptional effects of hydrazide-hydrazones.

Materials and methods

Organic solvents, a collection of acyl hydrazide and carbonyl reagents, cell culture media and other reagents, TLC plates and cell culture plasticware were purchased from Thermo Scientific or Millipore-Sigma vendors. All reagents were used without purification. Nifuroxazide was from Millipore-Sigma (cat. #481984500MG); human recombinant interleukin-1 β (PeproTech cat. #200–01B), human recombinant interleukin-6 (PeproTech cat. #200–06), human recombinant

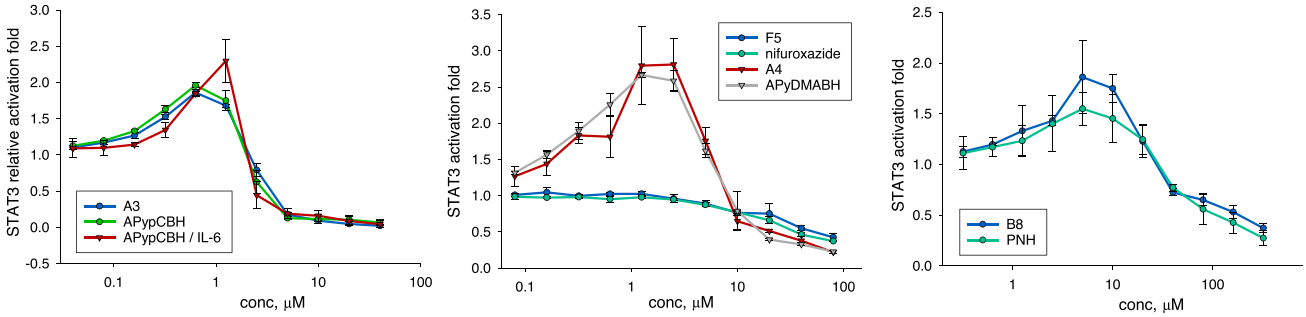

Fig. 7 Dose-response curves for transcriptional activity of the STAT3 reporter in THP-1 monocytes treated with the **A3**, **A4**, **B8**, and **F5** combinations and matching synthetic hydrazide-hydrazones APypCBH, APyDMABH, PNH, and nifuroxazide. In one case (left panel) the cells were also treated with combinations of 240 pM IL-6 and synthetic APypCBH; the relative STAT3 activation fold was calculated as luciferase activity in wells treated with the combinations divided by luciferase activity in wells treated with IL-6 alone. The error bars are SDs, $n = 3$

interferon-α1b (GenScript cat. #Z02866), and human recombinant GM-CSF (Shenandoah Biotech cat. #100-08 s) were purchased from Thermo Scientific.

Assembly of the combinatorial library

Stock solutions of 10 acyl hydrazides and 7 carbonyls were prepared in 1:4 (v:v) DMSO/propyleneglycol at 20 mM concentration. The carbonyl/hydrazide combinations of equal 100 µL volumes were arranged in the 96-well plate format and kept in strips of closed polypropylene PCR tubes for 1–6 h, until completeness of the reactions, as evidenced by TLC on silica gel. Immediately before addition to cells, the stock solutions were diluted in the experimental cell culture media to desired concentrations.

Syntheses of hydrazide-hydrazones

2-Acetylpyridine 4-chlorobenzoylhydrazone

p-Chlorobenzoic hydrazide (171 mg, 1 mmole) and 2-acetylpyridine (112 µL, 1 mmole) in 5 mL 95% EtOH were completely dissolved, then 200 µL 5 N HNO_3 were added and the solution was heated at 70 °C for 10 min. Crystallization started during heating. The reaction mixture was allowed to stand at room temperature for 18 h, washed with cold ethanol and dried *in vacuo*. From this crop, crystals was taken for further X-ray diffraction studies. Yield 252 mg (71%) of 2-acetylpyridine 4-chlorobenzoylhydrazone hydronitrate monohydrate (**1**). Analysis. Calc. for $C_{14}H_{13}N_4O_4Cl \times H_2O$: N, 15.79%; found: N, 15.78%. Exact mass of the $[M + H]^+$ ion. Calc. for $C_{14}H_{13}N_3OCl$: m/z 274.07 (100.0%), 276.07 (32.0%), 275.08 (15.1%). Found: m/z 274.01 (100.0%), 276.02 (35%), 275.03 (19%). See Fig. 6, S11 and Table 1, S1-S3 for exact molecular structure and crystal parameters.

2-Acetylpyridine 4-dimethylaminobenzoylhydrazone

4-Dimethylaminobenzhydrazide (358 mg, 2 mmoles) and 2-acetylpyridine (224 µL, 2 mmole) in 15 mL 95% EtOH/MeOH (2:1, v/v) were completely dissolved, then 333 µL 6 N HCl were added and the solution was heated at 70 °C for 30 min. The reaction mixture was kept at 4 °C for 4 days, the resulting dark orange crystals were washed with ice-cold ethanol and dried *in vacuo*. Yield 354 mg (46%) of 2-acetylpyridine 4-dimethylaminobenzoylhydrazone hydrochloride dihydrate MeOH solvate (**2**). Analysis. Calc. for $C_{16}H_{19}N_4OCl \times 2H_2O$: N, 15.79%; found: N, 15.52%. Exact mass of the $[M + H]^+$ ion. Calc. for $C_{16}H_{19}N_4O$: m/z 283.16 (100.0%), 284.16 (17.6%). Found: m/z 283.08 (100.0%), 284.09 (17.5%). See Fig. 6, S12 and Table 1, S4–S6 for exact molecular structure and crystal parameters.

Pyridoxal nicotinoylhydrazone

Solutions of nicotinoylhydrazide (137 mg, 1 mmole) in 5 mL 95% EtOH and pyridoxal hydrochloride (207 mg, 1 mmole) in 400 µL H_2O were combined and left to crystallize at room temperature. The resulting dense crystalline mass was recrystallized from 10 mL MeOH, washed with ice-cold ethanol and dried in vacuo. Yield 125 mg (37%) of pyridoxal nicotinoylhydrazone hydrochloride monohydrate (**3**). Analysis. Calc. for $C_{14}H_{15}N_4O_3Cl \times H_2O$: N, 16.44%; found: N, 16.53%. Exact mass of the $[M + H]^+$ ion. Calc. for $C_{14}H_{15}N_4O_3$: m/z 287.11 (100.0%), 288.12 (15.4%). Found: m/z 287.08 (100.0%), 288.08 (16%). See Fig. 6, S13 and Table 1, S–S9 for exact molecular structure and crystal parameters.

X-ray diffraction studies

Crystal data and experimental details of the crystallographic studies are given in Table 1, S1–S9. The crystal structures were solved with the direct methods program SHELXS and

refined by full-matrix least squares techniques using the SHELXL suite of programs [33], with the help of Olex2 [34]. Data were corrected for Lorentz, polarization, and absorption effects. Non-hydrogen atoms were refined with anisotropic thermal parameters. The hydroxyl and ammonium hydrogen atoms were located in difference Fourier maps and were allowed to refine freely. The remaining H atoms were placed at calculated positions and included in the refinement using a riding model. All hydrogen atom thermal parameters were constrained to ride on the carrier atoms (U_{iso}(methine, methylene H) = 1.2 U_{eq} and U_{iso}(hydroxyl, ammonium H) = 1.5 U_{eq}). Structure visualization was carried out with the Mercury program [35].

Signaling pathway reporters

Super *piggyBac* transposase expression vector PB210PA-1 was purchased from System Biosciences. The preparation and validation of reporter plasmids carrying insulated *piggyBac* transposon constructs, which contain transcriptional response element (TRE) and reporter genes, firefly luciferase, and a copepod green fluorescent protein (cGFP), as shown in Fig. 1, were reported earlier [18–20].

Cell culture

Human monocyte-macrophage cell line THP-1 [36] has been purchased from the American Type Culture Collection (ATCC). The original cells, as well as the THP-1 based reporter transfects, have been routinely cultured in RPMI-1640 medium (Sigma) supplemented with 10% heat-inactivated FBS (HyClone), additional 2 g/L glucose, 1 mM sodium pyruvate, 10 mM HEPES (both from Sigma), and 1% penicillin/streptomycin cocktail (pen/strep, CellGro). The cell density was maintained between 1×10^5 and 1×10^6 cell/ mL.

Human hepatocellular carcinoma line HepG2 and murine embryonic fibroblasts NIH 3T3 were obtained from the ATCC. HepG2, NIH 3T3, and their reporter cell lines for the STAT3 activation have been routinely cultured in 1:1 DMEM/F12 Ham (Sigma-Millipore) media supplemented with 5% newborn calf serum (NCS, HyClone) and 1% (v/v) pen/strep. This medium is henceforth referred to as the DMEM/F12 complete medium. To passage, the cells were treated with 0.05% trypsin (MP Biochemicals) in 1:1 Corning CellStripper cocktail/PBS (Sigma-Millipore) and subcultured at 1:5 ratio upon reaching near confluency.

The standard culturing conditions for all cells were 37 °C, 5% CO_2, and 100% humidity.

Stable transfections

Generation of THP-1 based stable reporter cell lines for the NF-κB, Nrf2, and HIF-1α transcriptional activation has been described earlier [18]. To perform stable transfection of the reporter plasmids for the STAT3 and MTF-1 transcriptional activation [19, 20], the original THP-1 cells were seeded into wells of a 96-well plate, at 5×10^5 cells per well in antibiotic-free 300 µL RPMI-1640, supplemented with 5% heat-inactivated FBS and 1% of the NATE inhibitor cocktail (InVivoGen). After 30 min, the cells were treated with a mixture of 100 ng of a reporter plasmid and 33 ng Super *piggyBac* transposase plasmid complexed with TransIT X2 transfection reagent (Mirus) at 1:2 (µg DNA/ µL) ratios. After 16 h, the regular media were added and the cells were left to proliferate for next 48–72 h. The transfected cells were then treated with the selecting antibiotic (5 µg/mL puromycin) for another week, and the surviving cells were expanded for cryopreservation and activity validation. Stable reporters of the STAT3 activation in HepG2 and NIH 3T3 cells were generated in the similar way, except these cell lines were adherent, at 2×10^5 cells per well in complete DMEM/F12 media, and did not require the NATE inhibitor treatment.

Cell treatment schedules

In a typical experiment, reporter monocyte THP-1 cells were adapted to a low serum medium, RPMI-1640 medium supplemented with 2 mg/L insulin, 2 mg/L transferrin, 2 µg/L selenite (2-ITS), 4% NCS, and the pen/strep antibiotic. After 40 h, the adaptation medium was replaced with the Phenol Red-free 5:5:1 DMEM/F12 Ham/RPMI-1640 mixture, supplemented with 1 g/L BSA, the 2-ITS mix and the pen/strep (the test medium). The cells were cultured for next 6 h, then seeded into wells of a 96-well U-bottom plate, at 5×10^4 cells per well in fresh test medium, now containing standards or synthetic test agents.

To obtain a macrophage phenotype, THP-1 cells were suspended in Serum-free Macrophage Medium (Lonza) containing 2 ng/mL phorbol myristate acetate (PMA) and seeded at 5×10^5 cells per well in a 96-well flat-bottom plate. After 48 h, the differentiation medium was replaced with the test medium. The THP-1 macrophages were cultured for next 6 h, followed by addition of standards or synthetic test agents.

HepG2 and NIH 3T3 cells were seeded at 1.5×10^4 cells/ well in 100 µL of an adaptation low-serum medium, which consisted of the DMEM/F12 media mixture supplemented with 2% NCS, 2-ITS, and the pen/strep antibiotic. After 40 h, the adaptation medium was replaced with the test medium, the cells were cultured for next 6 h, followed by addition of standards or synthetic test agents.

The experimental treatments lasted, unless specified, 18 h in standard conditions (37 °C, 100% humidity and 5% CO_2).

Transcriptional activity reporter assay

Immediately after the treatments, the reporter cells in 96-well plates were carefully washed with PBS and lysed in 70 µL of the lysing buffer [19] for 16 h at 8 °C. The lysates GFP fluorescence was measured at the 482(9)/512(17) nm wavelength (slit width) setup; this was followed by an addition of 20 µL the luciferase substrate [19], and kinetic luminescence readings in the wells were done in 2 min intervals for 8 min total. All measurements were done using a Synergy MX (BioTek) plate reader. The GFP fluorescence values were used for both evaluation of relative cell transcriptional/translational activity/proliferation and normalization of the reporter luciferase activities in respective wells [18].

Plotting and statistical analysis

Statistical tests and plots were done using SigmaPlot, version 13.0

Funding This research was supported, in part, by the University of Missouri Experiment Station Chemical Laboratories and the USDA National Institute of Food and Agriculture, Hatch project 1023929.

Compliance with ethical standards

Conflict of interest The authors declare no conflict of interest.

References

1. Eder J, Sedrani R, Wiesmann C. The discovery of first-in-class drugs: origins and evolution. Nat Rev Drug Disco. 2014;13:577–87. https://doi.org/10.1038/nrd4336
2. Scannell JW, Blanckley A, Boldon H, Warrington B. Diagnosing the decline in pharmaceutical R&D efficiency. Nat Rev Drug Disco. 2012;11:191–200. https://doi.org/10.1038/nrd3681
3. Tang J, Tanoli Z-u-R, Ravikumar B, Alam Z, Rebane A, Vaha-Koskela M, et al. Drug target commons: a community effort to build a consensus knowledge base for drug-target interactions. Cell Chem Biol. 2018;25:224–9 e2. https://doi.org/10.1016/j.chembiol.2017.11.009
4. Pushpakom S, Iorio F, Eyers PA, Escott KJ, Hopper S, Wells A, et al. Drug repurposing: progress, challenges and recommendations. Nat Rev Drug Disco. 2019;18:41–58. https://doi.org/10.1038/nrd.2018.168
5. Johnson DE, O'Keefe RA, Grandis JR. Targeting the IL-6/JAK/STAT3 signalling axis in cancer. Nat Rev Clin Oncol. 2018;15:234–48. https://doi.org/10.1038/nrclinonc.2018.8
6. Grivennikov SI, Karin M. Dangerous liaisons: STAT3 and NF-κB collaboration and crosstalk in cancer. Cytokine Growth Factor Rev. 2010;21:11–9. https://doi.org/10.1016/j.cytogfr.2009.11.005
7. Yu H, Kortylewski M, Pardoll D. Crosstalk between cancer and immune cells: role of STAT3 in the tumour microenvironment. Nat Rev Immunol. 2007;7:41–51. https://doi.org/10.1038/nri1995
8. Mohan CD, Rangappa S, Preetham HD, Chandra Nayaka S, Gupta VK, Basappa S, et al. Targeting STAT3 signaling pathway in cancer by agents derived from mother nature. Semin Cancer Biol. 2022;80:157–82. https://doi.org/10.1016/j.semcancer.2020.03.016
9. Thilakasiri PS, Dmello RS, Nero TL, Parker MW, Ernst M, Chand AL. Repurposing of drugs as STAT3 inhibitors for cancer therapy. Semin Cancer Biol. 2021;68:31–46. https://doi.org/10.1016/j.semcancer.2019.09.022
10. Nelson EA, Walker SR, Kepich A, Gashin LB, Hideshima T, Ikeda H, et al. Nifuroxazide inhibits survival of multiple myeloma cells by directly inhibiting STAT3. Blood. 2008;112:5095–102. https://doi.org/10.1182/blood-2007-12-129718
11. Zhu Y, Ye T, Yu X, Lei Q, Yang F, Xia Y, et al. Nifuroxazide exerts potent anti-tumor and anti-metastasis activity in melanoma. Sci Rep. 2016;6:20253 https://doi.org/10.1038/srep20253
12. Gan C, Zhang Q, Liu H, Wang G, Wang L, Li Y, et al. Nifuroxazide ameliorates pulmonary fibrosis by blocking myofibroblast genesis: a drug repurposing study. Respir Res. 2022;23:32 https://doi.org/10.1186/s12931-022-01946-6
13. Wang Y, Liu W, Liu M, Wang H, Zhou L, Chen J, et al. Nifuroxazide in combination with CpG ODN exerts greater efficacy against hepatocellular carcinoma. Int Immunopharmacol. 2022;108:108911 https://doi.org/10.1016/j.intimp.2022.108911
14. Said E, Zaitone SA, Eldosoky M, Elsherbiny NM. Nifuroxazide, a STAT3 inhibitor, mitigates inflammatory burden and protects against diabetes-induced nephropathy in rats. Chem-Biol Interact. 2018;281:111–20. https://doi.org/10.1016/j.cbi.2017.12.030
15. Thota S, Rodrigues DA, Pinheiro PDSM, Lima LM, Fraga CAM, Barreiro EJ. N-Acylhydrazones as drugs. Bioorg Med Chem Lett. 2018;28:2797–806. https://doi.org/10.1016/j.bmcl.2018.07.015
16. Kajal A, Bala S, Sharma N, Kamboj S, Saini V. Therapeutic potential of hydrazones as anti-inflammatory agents. Int J Med Chem. 2014;761030/1-/12:12 https://doi.org/10.1155/2014/761030
17. Wahbeh J, Milkowski S. The use of hydrazones for biomedical applications. SLAS Technol. 2019;24:161–8.
18. Mossine VV, Waters JK, Hannink M, Mawhinney TP. *piggyBac* Transposon plus insulators overcome epigenetic silencing to provide for stable signaling pathway reporter cell lines. PLoS One. 2013;8:e85494.
19. Mossine VV, Waters JK, Gu Z, Sun GY, Mawhinney TP. Bidirectional responses of eight neuroinflammation-related transcriptional factors to 64 flavonoids in astrocytes with transposable insulated signaling pathway reporters. ACS Chem Neurosci. 2022;13:613–23. https://doi.org/10.1021/acschemneuro.1c00750
20. Mossine VV, Waters JK, Chance DL, Mawhinney TP. Transient proteotoxicity of bacterial virulence factor pyocyanin in renal tubular epithelial cells induces ER-related vacuolation and can be efficiently modulated by iron chelators. Toxicol Sci. 2016;154:403–15.
21. Bernhardt PV, Wilson GJ, Sharpe PC, Kalinowski DS, Richardson DR. Tuning the antiproliferative activity of biologically active iron chelators: characterization of the coordination chemistry and

biological efficacy of 2-acetylpyridine and 2-benzoylpyridine hydrazone ligands. JBIC J Biol Inorg Chem. 2008;13:107–19. https://doi.org/10.1007/s00775-007-0300-4
22. Triner D, Shah Yatrik M. Hypoxia-inducible factors: a central link between inflammation and cancer. J Clin Invest. 2016;126:3689–98.
23. Maxwell P, Salnikow K. HIF-1: an oxygen and metal responsive transcriptional factor. Cancer Biol Ther. 2004;3:29–35. https://doi.org/10.4161/cbt.3.1.547
24. Hübner C, Haase H. Interactions of zinc- and redox-signaling pathways. Redox Biol. 2021;41:101916 https://doi.org/10.1016/j.redox.2021.101916
25. Bellezza I, Mierla AL, Minelli A. Nrf2 and NF-κB and their concerted modulation in cancer pathogenesis and progression. Cancers. 2010;2:483–97. https://doi.org/10.3390/cancers2020483
26. Baens M, Noels H, Broeckx V, Hagens S, Fevery S, Billiau AD, et al. The dark side of EGFP: defective polyubiquitination. PLoS One. 2006;1:e54 https://doi.org/10.1371/journal.pone.0000054
27. Lovejoy DB, Richardson DR. Iron chelators as anti-neoplastic agents: current developments and promise of the PIH class of chelators. Curr Med Chem. 2003;10:1035–49. https://doi.org/10.2174/0929867033457557
28. Haskova P, Kovarikova P, Koubkova L, Vavrova A, Mackova E, Simunek T. Iron chelation with salicylaldehyde isonicotinoyl hydrazone protects against catecholamine autoxidation and cardiotoxicity. Free Radic Biol Med. 2011;50:537–49. https://doi.org/10.1016/j.freeradbiomed.2010.12.004
29. Cho EA, Song HK, Lee S-H, Chung BH, Lim HM, Lee MK. Differential in vitro and cellular effects of iron chelators for hypoxia inducible factor hydroxylases. J Cell Biochem. 2013;114:864–73. https://doi.org/10.1002/jcb.24423
30. Pniewska B, Januchowski M. Structural investigations of nifuroxazide, p-hydroxy-N'-(5-nitrofurfurylidene)benzhydrazide. Pol J Chem. 1998;72:2629–34.
31. Covaci O-I, Mitran R-A, Buhalteanu L, Dumitrescu DG, Shova S, Manta C-M. Bringing new life into old drugs: a case study on nifuroxazide polymorphism. Cryst Eng Comm. 2017;19:3584–91. https://doi.org/10.1039/c7ce00303j
32. Jia H, Cui J, Jia X, Zhao J, Feng Y, Zhao P, et al. Therapeutic effects of STAT3 inhibition by nifuroxazide on murine acute graft graft-vs.-host disease: old drug, new use. Mol Med Rep. 2017;16:9480–6. https://doi.org/10.3892/mmr.2017.7825
33. Sheldrick GM. Crystal structure refinement with SHELXL. Acta Crystallogr. 2015;C71:3–8. https://doi.org/10.1107/s2053229614024218
34. Dolomanov OV, Bourhis LJ, Gildea RJ, Howard JAK, Puschmann H. OLEX2: a complete structure solution, refinement and analysis program. J Appl Crystallogr. 2009;42:339–41. https://doi.org/10.1107/s0021889808042726
35. Macrae CF, Bruno IJ, Chisholm JA, Edgington PR, McCabe P, Pidcock E, et al. Mercury CSD 2.0 - new features for the visualization and investigation of crystal structures. J Appl Crystallogr. 2008;41:466–70. https://doi.org/10.1107/s0021889807067908
36. Auwerx J. The human leukemia cell line, THP-1: a multifacetted model for the study of monocyte-macrophage differentiation. Experientia.1991;47:22–31.
37. Parsons S, Flack HD, Wagner T. Use of intensity quotients and differences in absolute structure refinement. Acta Crystallogr. 2013;B69:249–59. https://doi.org/10.1107/s2052519213010014